



A microfluidic device for real-time on-demand intravenous oxygen delivery

Ashwin Kumar Vutha^{a,b}, Ryan Patenaude^b, Alexis Cole^b, Rajesh Kumar^{a,b} , John N. Kheir^{a,b}, and Brian D. Polizzotti^{a,b,c,1} 

Edited by Robert Austin, Princeton University, Princeton, NJ; received August 18, 2021; accepted January 25, 2022

Oxygen is picked up in the lungs, carried by the blood, and delivered to tissues where it serves as the terminal electron acceptor during oxidative phosphorylation. During health, oxygen is available in abundance; however, COVID-19 and many other forms of critical illness can damage the lungs and compromise systemic oxygen delivery. Cells that are very active cannot tolerate deficiencies in energy production that result from oxygen deprivation. Hypoxemia that lasts even a few minutes can turn a healthy person into a neurologically devastated patient for life, and when refractory it is often lethal. In this paper, we develop a way to administer oxygen gas to a patient through an intravenous line, replacing or supplementing the function of injured lungs. Here, we show that by coinfusing oxygen gas and a liquid solution through a series of sequential nozzles of decreasing size we are able to create bubbles of oxygen that are smaller than a single red blood cell on demand and in real time. These bubbles are coated with a “membrane” similar to that in every other cell in the body, which 1) prevents them from merging with other bubbles to create larger ones, 2) provides a path for oxygen to diffuse out and into the blood, and 3) minimizes the likelihood of material-related toxicities. Importantly, these devices allow us to control the dosage of oxygen delivered and the volume of fluid administered, both of which are critical parameters in the management of critically ill patients.

hypoxia | nanospray | oxygen | nanobubbles | intravenous

Hypoxia is an important cause of morbidity and mortality. Hypoxia may occur as a result of acute lung injury (e.g., blast injury or acute respiratory distress syndrome [ARDS]), airway obstruction (e.g., facial trauma), COVID-19 infection, or chronic lung disease, among others. Treatment of patients with refractory hypoxia is challenging, requiring intubation and mechanical ventilation, transport to tertiary care centers, and prolonged intensive care. Extended mechanical ventilation and high concentrations of inspired oxygen may compound lung injury (i.e., ventilator-induced lung injury), such that the most hypoxic patients experience the most compounding injury. The ability to directly supplement oxygenation via the intravenous route may significantly improve patient stability during transport and may diminish ventilator-related lung injury in patients suffering from refractory hypoxic respiratory failure.

Our group has found that oxygen gas can be safely injected intravenously if it is packaged into microparticles which contain the gas and prevent coalescence within the vascular system (Fig. 1) (1, 2). We found that partitioning the gas into 2- to 4- μm -diameter microparticles allows them to easily pass through the circulation without causing obstruction and provides a large surface area-to-volume ratio for rapid gas exchange. We have also found that the choice of shell material plays a critical role in defining the microparticle behavior (3, 4)—and hence its clinical potential to provide both short- and long-term oxygen support (1, 2, 5–7). Patients with respiratory failure may take weeks to recover, such that infusions of oxygen would ideally be long-term and the toxicities of the shell material play a prominent role in the choice of microparticle. Of the materials we have studied, lipid oxygen microparticles (LOMs; Fig. 1, Generation 1) are favorable for several reasons. First, they are the most biomimetic (8); the lipids used to stabilize LOMs are similar in structure to those found in cell membranes and do not elicit shell-related toxicities even following prolonged administration at high concentrations (9). In fact, intravenous injection of lipid emulsions is routinely used as an energy source in critically ill patients (e.g., the usual lipid dosage of Intralipid 20% is ~ 6 g lipid per day for a 70-kg adult) (10). Second, LOMs minimize the volume of material required for administration of a given volume of gas. In contrast to polymer-based shells (that we are still developing for more emergent clinical scenarios), phospholipids create an angstrom-thick monolayer at the gas–fluid interface (11); the minimum thickness of our polymer shells is ~ 50 nm, an order of magnitude higher (12). Third, circulating LOMs are malleable, deforming for passage through capillaries

Significance

The treatment of hypoxemia that is refractory to the current standard of care is time-sensitive and requires skilled caregivers and use of specialized equipment (e.g., extracorporeal membrane oxygenation). Most patients experiencing refractory hypoxemia will suffer organ dysfunction, and death is common in this cohort. Here, we describe a new strategy to stabilize and support patients using a microfluidic device that administers oxygen gas directly to the bloodstream in real time and on demand using a process that we call sequential shear-induced bubble breakup. If successful, the described technology may help to avoid or decrease the incidence of ventilator-related lung injury from refractory hypoxemia.

Author affiliations: ^aDepartment of Pediatrics, Harvard Medical School, Boston, MA 02115; ^bDepartment of Cardiology, Boston Children's Hospital, Boston, MA 02115; and ^cExperimental Therapeutics Program, Dana Farber Cancer Institute/Harvard Cancer Center, Boston, MA 02215

Author contributions: A.K.V. and B.D.P. designed research; A.K.V. designed and manufactured the device; A.K.V., R.P., A.C., R.K., J.N.K., and B.D.P. performed research; A.K.V. and B.D.P. analyzed data; B.D.P. wrote the paper; and all authors edited the paper.

The authors declare no competing interest.

This article is a PNAS Direct Submission.

Copyright © 2022 the Author(s). Published by PNAS. This article is distributed under [Creative Commons Attribution-NonCommercial-NoDerivatives License 4.0 \(CC BY-NC-ND\)](https://creativecommons.org/licenses/by-nc-nd/4.0/).

¹To whom correspondence may be addressed. Email: brian.polizzotti@gmail.com.

This article contains supporting information online at <http://www.pnas.org/lookup/suppl/doi:10.1073/pnas.2115276119/-/DCSupplemental>.

Published March 21, 2022.

	GENERATION I Phospholipid DSPC	GENERATION II Polymeric nanoporous PLGA	GENERATION III Composite triggered BD shell DASH
BENEFITS	↑ Gas fraction Rapid dissolution	Manufacture control Shelf stability Pressurizable Customizable gas release	↑ Gas fraction Manufacture control Circulating oncotic agent Shelf stability Stored ready to inject
DRAWBACKS	Poor shelf stability Poor manufacture control Gas embolism	↓ Gas fraction Shell persistence → dose limiting Stored as powder	Transient mild thrombocytopenia
OPTIMIZATIONS	Viscosity Stability Surface coating	Shell porosity Shell thickness Core pressure	Degree of acetylation
TESTING	Safety (Rats) Reversal of hypoxia (Rabbits) Efficacy in preventing ACA (Rabbits) ↑ DO ₂ in cardiac arrest (Swine)	Safety (Rats) Reversal of hypoxia (Rats) Hemorrhagic shock (Rats)	Safety (Rats) Efficacy in treating ACA (Rats) Long-term safety (Swine)

Fig. 1. Our group has developed and tested three major generations of oxygen-filled microparticles, each with defined benefits and drawbacks as an injectable oxygen carrier. DSPC = 1,2-distearoyl-sn-glycero-3-phosphocholine; PLGA = poly(lactic-co-glycolic acid); DASH = dextran acetate succinate (with a high degree of substitution); ACA = asphyxial cardiac arrest; DO₂ = oxygen delivery.

and shedding small micelles as the internal volume decreases, preventing vascular obstruction during prolonged administration (11). Fourth, LOMs can be concentrated to greater than 70% gas by volume, thus minimizing the volume of fluid that must be administered (13). The challenge with LOMs, however, is that they are structurally weak. Unlike polymeric shells, LOMs are inherently unstable and may burst, grow, or dissolve depending on their local environment (14–17). For example, we have shown that prolonged storage of concentrated LOMs at room temperature results in a significant decrease in the total gas fraction (resulting in substantial formation of lipid contaminate) and an increase in the mean bubble diameter of surviving bubbles (18). Although this was improved somewhat with storage at cold temperatures, intravenous injection of refrigerated LOMs after 30 d of storage was lethal to healthy animals (18). We have also shown that during rapid injection LOMs burst due to the overpressure, leading to the formation of macrobubbles within major blood vessels, causing pulmonary embolism and death (19). Although we explored the possibility of enhancing the strength of LOMs by utilizing electrostatic coatings, the use of viscosity-enhancing reagents (7), and chemical cross-linking of the lipid membrane, these approaches proved largely ineffective. Given the unmatched benefits of LOMs for long-term intravenous oxygen delivery, we created a microfluidic device that enables on-demand and real-time production of lipidic microbubbles with controlled particle size, tunable gas fractions, and volumetric flow rates.

Results

Our device uses a flow-focusing geometry and includes 1) a step change in the first channel to reduce the pressure drop requirement (20) and to trigger initial bubble formation and 2) additional nozzles downstream of the two-phase junction, which uses velocity-induced shear forces to sequentially break down macrobubbles into micrometer- and nanometer-sized bubbles. We systematically varied the number, placement, and dimensions of both the step changes and the nozzles (*SI Appendix, Figs. S1–S4*) and evaluated their ability to stably spray oxygen nano/microbubbles at the required volumetric

flow rates [e.g., 0.05 to 0.5 mL O₂/min or ~1 to 10% of the baseline oxygen consumption of Sprague-Dawley rats; we have previously demonstrated that delivering ~0.5 mL O₂/min or 10% VO₂ was sufficient to resuscitate rats from 10 min of asphyxia leading to cardiac arrest (21)]. We found that the optimal device geometry had an oversized nozzle at the two-phase junction (120 μm) followed by an immediate step change in channel depth from 30 μm to 55 μm (Fig. 2*B*) and three sequential in-line nozzles, each with progressively smaller openings (20 μm, 20 μm, and 15 μm; Fig. 2*A* and *C* and *SI Appendix, Figs. S5* and *S6*). Using this geometry, we show that for a given liquid flow rate Q_l, increasing the gas flow rate Q_g from 0.125 to 0.7 mL O₂/min results in a gradual increase in the gas pressure, which eventually stabilized (Fig. 3*A* and *SI Appendix, Fig. S7*). Importantly, we found that achieving steady state was critical to spraying bubbles with narrow size distributions (Fig. 3*B*). We found that for a given liquid flow rate, increasing the gas flow rate above 0.125 mL O₂/min resulted in an increase in the concentration of nano- and microbubbles (e.g., increasing from 0.25 to 0.7 mL O₂/min resulted in a 2.5-fold increase in the concentration of nanobubbles; 3.5 × 10⁴ bubbles/mL vs. 8.6 × 10⁴ bubbles/mL, *P* < 0.0001; Fig. 3*B* and *SI Appendix, Fig. S8*), with greater than 90% and 95% of all bubbles being less than 10 μm and 12 μm, respectively (approximating the diameter of circulating red blood cells). The control lipid solution showed negligibly low bubble concentrations. It is worth highlighting that bubble coalescence within bulk water occurs within milliseconds, such that these values are likely to be overestimates of the true size distribution of the bubbles infused during intravenous administration. Also noteworthy, we found that the average bubble diameter showed only a weak dependence at higher liquid flow rates, which makes scaling the device more feasible; similar results have been observed for traditional flow-focusing generators (22). When examined in vitro, our devices raised the oxygen saturation (SO₂) of deoxygenated human blood from 15 to >95% within seconds to minutes depending on Q_g (effective concentration at 95% saturation, EC₉₅ = 25.94 s, 37.96 s, and 137.6 s for Q_g = 0.7, 0.4, and 0.25 mL O₂/min, respectively; Fig. 4*A* and *SI Appendix, Fig. S9*) and effectively delivered between 80 to

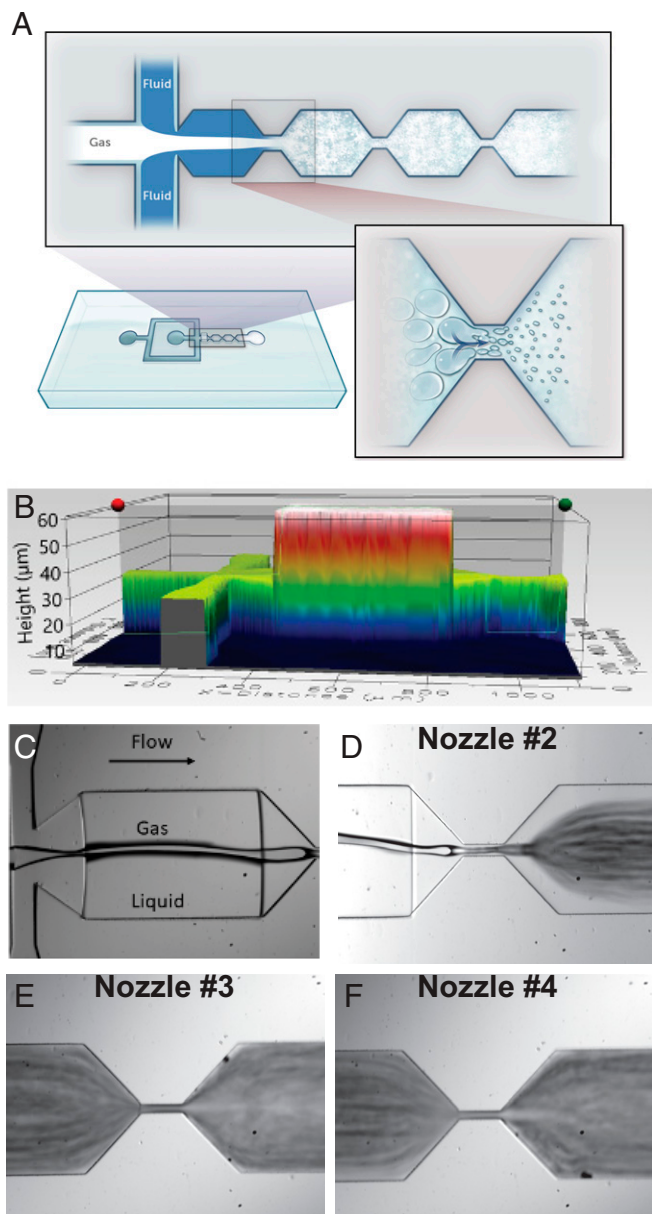


Fig. 2. (A) Schematic of the device geometry illustrating the bubble breakup mechanism. (B) Three-dimensional optical profilometry measurement of the SU-8 mold used to fabricate the microdevices. (C–F) Optical micrographs of the nanospraying process. As the liquid and gas phases enter the junction nozzle, the liquid phase focuses the gas into a jet (C). Once the gas jet enters the second nozzle, the liquid phase becomes atomized into microbubbles (D). Subsequent passage through nozzles #3 (E) and #4 (F) use velocity-induced shear to further reduce the bubble size.

95% of the administered oxygen (estimated by $Q_g \times \text{time}$ needed to reach saturation; Fig. 4B).

We next examined the acute safety of the microdevices during intravenous oxygen delivery as a function of gas flow rates (Q_g was kept constant at 12 mL/h). In $n = 9$ healthy rats ($n = 3$ per group), instrumented to allow real-time monitoring of hemodynamic data, there were no significant changes in major hemodynamic parameters 1 h after oxygen was continuously infused for 30 min at flow rates of 0.0, 0.25, and 0.4 mL O_2 /min (equivalent to 0%, 5%, and 8% VO_2 , respectively). However, we found evidence of vascular obstruction (e.g., increased pulmonary vascular resistance [PVR]) when Q_g was raised to 0.7 mL O_2 /min (equivalent to 14% VO_2 ; Fig. 5A). We observed that the right ventricle (RV) became visibly

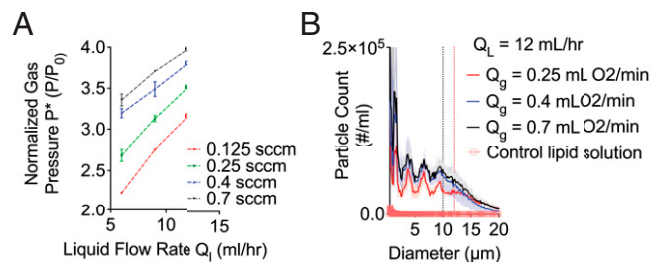


Fig. 3. (A) Normalized steady-state gas pressure as a function of liquid flow rate. (B) The size distribution nano/microbubbles as a function of increasing oxygen flow rate at a $Q_l = 12$ mL/h.

distended over time, suggesting that the rate of oxygen delivery exceeded the local sink conditions, resulting in microbubble coalescence and vascular obstruction (*SI Appendix*, Fig. S10) (23). This likely reflects inherent limitations in the safety model (i.e., absence of severe arterial hypoxemia) and is not an accurate measure of the maximum tolerated dose (i.e., intravenous administration of oxygen gas at 0.7 mL O_2 /min may be well-tolerated in animals suffering from ARDS). Finally, necropsy revealed no evidence of acute lung injury nor a significant interaction with any blood components (as evidenced by lack of blood clot formation) when infused at rates up to 0.4 mL O_2 /min (*SI Appendix*, Fig. S11).

To demonstrate efficacy in providing supplemental oxygenation, venous oxygen tension (PvO_2) was measured continuously in the RV of healthy animals using an implantable oxygen electrode. This model is clinically relevant in that the mechanism by which patients with respiratory failure due to COVID-19, for example, become hypoxemic is intrapulmonary shunting—instead of becoming reoxygenated in the lungs, blood passes from the pulmonary artery to the pulmonary vein (and subsequently the body) without gas exchange, creating arterial hypoxemia (24). Following a 30-min baseline period, in the same experimental construct, oxygen gas was administered intravenously via the microdevices at either 0.0, 0.25, or 0.4 mL O_2 /min for 30 min (at a constant fluid flow rate of 12 mL/min) followed by a 90-min observation period. Animals treated with intravenous oxygen exhibited dose-dependent increases in venous oxygen saturation which peaked at 30 min and gradually returned to baseline, observations that were lower in the control group (i.e., animals treated with fluid only; Fig. 5B). The peak change in PvO_2 (percent change from baseline) increased from 9.92% for controls to 20.04% and 34.14% ($P < 0.05$) for $Q_g = 0.25$ and 0.4 mL O_2 /min, respectively (Fig. 5C). We estimate that this equates to raising the arterial oxygen saturation by $\sim 20\%$ to $\sim 50\%$ (25), respectively, a clinically important quantity. This suggests that our microdevices may increase arterial oxygenation in an animal model of ARDS.

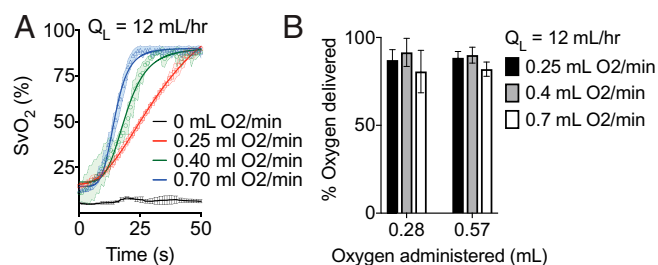


Fig. 4. (A) Increasing the oxygen flow rate decreases the time needed to reach saturation. (B) Spraying delivers ~ 80 to 95% of administered oxygen.

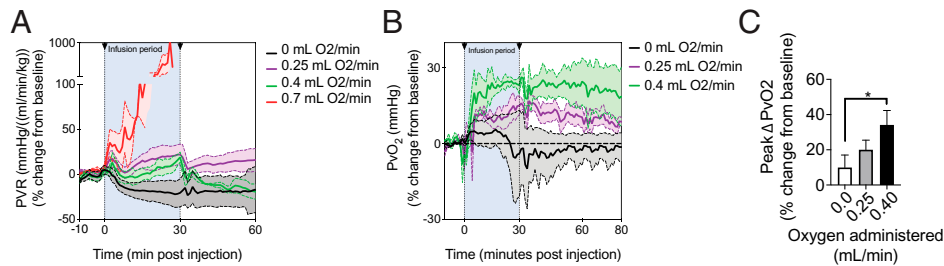


Fig. 5. Animals received either intravenous oxygen ($Q_I = 12$ mL/min; $Q_G = 0.25, 0.4,$ or 0.7 mL O₂/min) or oxygenated lipidic solution continuously for 30 min followed by a 60-min observation period. (A) The PVR was significantly higher in animals treated with 0.7 mL O₂/min, compared to other groups. (B) Intravenous nanospraying of oxygen bubbles transiently increased the PvO₂ in a dose-dependent manner. (C) Continuous intravenous infusion of oxygen at 0.4 mL O₂/min delivered significantly more oxygen gas than oxygen-saturated lipidic solution alone. * $P < 0.05$.

Discussion

Successfully delivering oxygen gas intravenously requires that one effectively titrate the oxygen delivery to match the oxygen sink within the blood stream. This requires real-time monitoring of hemodynamic parameters, e.g., blood saturation, blood pO₂, etc., and a way to rapidly regulate the concentration of oxygen being infused. Infusion of too little oxygen results in systemic hypoxia, and potentially death, whereas infusion of too much oxygen results in bubble coalescence and microvascular obstruction. There are several key attributes of the current device that may permit real-time regulation of these parameters, thus significantly enhancing the safety and efficacy of intravenous oxygen. First, the device generates a large fraction of nanobubbles (i.e., bubbles that are less than 1 μ m in diameter) that become consumed (i.e., deliver their gas payload) before they have a chance to grow in size (as opposed to using micrometer-sized bubbles produced via homogenization; *SI Appendix, Fig. S14*). Second, the device permits real-time regulation of the blood oxygen tension by varying the liquid (Q_L) and/or gas (Q_G) flow rates. This flexibility permits the safe infusion of low or high concentrations of oxygen gas ($\geq 90\%$ vol/vol) with minimal fluid, thus allowing one to reverse hypoxemia while avoiding hyperoxia. Admittedly, varying these parameters does lead to a transient instability in the nanospraying and requires that the flow be temporarily diverted (for several minutes) to avoid infusion of large macrobubbles, but this represents a minor engineering challenge that will be addressed in future generations. This is in stark contrast to infusion of a preformed microbubble solution, which requires higher infusion rates (and fluid volume) to increase the delivered oxygen content. The latter is especially important when treating patients with respiratory distress as they are particularly vulnerable to volume overload (i.e., in critically ill patients, one needs to minimize the volume of fluid administered while maximizing the oxygen content). Finally, it is worth mentioning that our device could potentially be integrated into existing ventilators, allowing for seamless integration into existing clinical workflows.

In conclusion, we have shown that clinically important volumes of oxygen gas ($\sim 20\%$ of baseline VO₂) can be delivered intravenously in real time by on-demand encapsulation within LOMs. It is clear that microbubbles are able to traverse the lung without causing obstruction and provide arterial oxygenation. Additionally, our design permits the devices to be parallelized to meet higher oxygen demand, if needed, and provides precise control over the oxygen and fluid delivery rates. This allows the target oxygen tension to be precisely titrated, reversing hypoxemia while avoiding hyperoxia (a major cause of oxygen toxicity and in vivo bubble coalescence). Importantly, in

situ oxygen-spraying LOMs minimizes concerns or shell-related toxicities and the need for long-term storage, which has long been a factor limiting clinical translation of microbubbles. We believe that the aforementioned effects would be particularly helpful in providing long-term oxygen support to patients with refractory hypoxic respiratory failure.

Materials and Methods

Microfluidic Device Design and Fabrication. The microfluidic devices used in this study were fabricated using standard lithography processes. A silicon mold was first fabricated in a cleanroom environment using SU-8 photoresist and masks that were designed using computer-aided design software. The three-dimensional expansion in the device was achieved using a second layer of photoresist spin-coated over the first and subsequent repetition of the downstream processes. The expansion was introduced to reduce the pressure drop requirement for pumping the two-phase mixture through the channel, an approach that has also been shown to aid the formation of submicron particles (22). Once the molds were fabricated, a homogenous mixture of polydimethylsiloxane (PDMS) prepolymer and curing agent in a 10:1 mass ratio was poured over the mold and cured for at least 6 h in a convection oven at 65 °C. The cured PDMS was then peeled off the wafer, diced into individual dies, and punched to create through holes for inlet and outlet ports. The dies were then cleaned extensively with solvents in an ultrasound bath, dried with N₂ gas, and baked overnight to eliminate residual solvents. The clean and dry dies were then treated with oxygen plasma (Microtechnik, 105 to 110 W, ~ 250 mTorr O₂) and bonded to clean glass slides. The ports for liquid and gas inlets were fitted with polytetrafluoroethylene (PTFE) tubing (Cole-Parmer Instrument Company, LLC) of ~ 1.6 mm outer diameter (O.D.) and inner diameter (I.D.) of ~ 800 μ m, and the corresponding dimensions for the outlet tubing (MSC Industrial Supply) were 800 μ m and 400 μ m, respectively.

Preparation of Lipid Solution. The lipid solution used as the carrier fluid for the oxygen bubbles was composed of distearoyl phosphatidylcholine (DSPC) (NOF America Corporation) at a concentration of 10 mg/mL and 2.8 mg/mL PEG40S (Sigma-Aldrich Corporation) in medical-grade saline (0.9%). The frozen dry lipid powder was first dissolved in chloroform which was stirred at 500 rpm and allowed to evaporate overnight. Lipid solution preparation in literature has typically involved the formation of a thin film of lipid on the inner wall of the container, followed by hydration of lipids and the use of ultrasound to break up the film and form a lipid suspension. Here, the lipid solution was prepared using a combination of a film and lipid agglomerates. Since a high-power tip sonicator (Branson Ultrasonics Corporation) was used to break up the lipids, the presence of lipid agglomerates was not a concern. In addition, the presence of free lipids in solution was observed to be beneficial for the formation of bubble foams at the relatively high flow rates employed in the devices. Once the chloroform had completely evaporated, a saline solution and PEG40S were then added to the beaker containing a dry lipid film as well as agglomerates of lipids. The solution was stirred at 500 rpm for 30 min, followed by treatment in a low-power ultrasound bath (Branson Ultrasonics Corporation) for up to 45 min. The beaker was then transferred to the high-power sonicator and subjected to ultrasound until a

translucent solution was obtained. This solution was refrigerated at 4 °C until ready for use. At the time of use the solution was at room temperature.

Experimental Setup and Size Analysis. A high-precision syringe pump (Harvard Bioscience, Inc.) was used to pump the liquid phase through the micro-channel (SI Appendix, Fig. S12). The gas was delivered from a compressed gas cylinder fitted with a two-stage regulator. A mass flow controller (Alicat Scientific, Inc.) was connected to the cylinder and used to regulate gas flow through the device. The lipid solution was loaded into a syringe which was then secured on to the syringe pump. PTFE tubing of 1.6-mm O.D. was then connected to the syringe using a blunt fill needle and the tubing was primed, before being inserted into the first inlet port of the device. Similarly, the tubing for the second (gas) inlet of the device and the 400- μ m-I.D. outlet tubing were thoroughly cleaned before being attached to the device. The operation of the device was extremely sensitive to contamination due to the small sizes of the nozzles and rigorous cleaning was required for all fluidic components of the experimental setup. The presence in the channel of any foreign particle on the order of the nozzle size was sufficient to obstruct flow and render the device unusable.

Once the device was integrated with the flow apparatus, gas flow through the device was initiated at the desired flow rate. The liquid flow was then triggered, starting at a very low value and incrementally increased. When the gas phase alone flows through the nozzles, the pressure increases above its atmospheric value due to the resistance offered by the channel. When liquid enters the channel, the space available to the gas is significantly reduced and the gas pressure further increases due to compressibility. The change in pressure to a new stable value is not instantaneous and occurs gradually over a significant time period, depending on the combination of gas and liquid flow rates. For each incremental change in liquid flow rate, a wait period was involved for the gas pressure to stabilize to a new higher value. Consequently, the liquid flow rate had to be increased gradually, to avoid inducing backflow of the liquid into the gas inlet, which would occur if the liquid pressure significantly exceeded that of the gas. The maximum liquid flow rate used in the experiments was chosen based on the stabilized value of gas pressure corresponding to the liquid flow rate. To avoid issues with delamination and failure of the device, the maximum liquid flow rate was limited to 12 mL/h, which led to a gas pressure of \sim 4 atm at the highest gas flow rate of 0.7 mL/min.

The device was allowed to operate at steady state for a few minutes prior to sample collection for size analysis. For collection of the sample, a scintillation vial was used with 2 mL of filtered deionized water as the diluent, for ease of collection of the foam. The outlet tube from the device was immersed in the water and the sample was collected for 60 s. The diluted sample was then injected into the measuring vessel of the optical sizing instrument, which further diluted the sample. The predilution process was accounted for in the measurement by specifying the predilution factor. At the end of a 60-s measurement a size distribution was obtained. This process was repeated three times ($n = 3$) for reproducibility at each combination of gas and liquid flow rate used in this study.

Oxygen Kinetic Studies. The *in vitro* assessment of the oxygenation capability of the microfluidic device was performed using desaturated donor human blood. To prepare the blood for the experiments, a small volume donated human red blood cells was diluted using Plasmalyte-A solution (pH = 7.4) until the Hgb concentration was between 13 g/dL and 15 g/dL. The pH of this blood was adjusted using sodium bicarbonate until it was in the range of 7.3 to 7.5. The above parameters were measured using an arterial blood gas analyzer (Radiometer America, Inc.). The blood was then warmed up to 37 °C on a plate with combined heating and stirring capabilities (Heidolph Instruments GmbH and Co. KG). To desaturate the blood, pressurized nitrogen gas was bubbled through the blood and periodic blood gas measurements were made, until the SO_2 dropped to \sim 10%. Simultaneously, the microfluidic device was set up as described in the previous section. Once the device was at steady state and the blood SO_2 had reached the desired value, a small volume of the blood (\sim 4.5 mL) was pipetted into a vial of the same volume containing micro stir bars, and the vial was placed on a stir plate. The stirring was increased to 1,000 rpm and the oximeter probe was immersed in the blood for a baseline SO_2 measurement. The outlet tubing from the microfluidic device was then immersed into the blood for a fixed time interval and the change in SO_2 was recorded. The maximum stable SO_2 value obtained was indicative of the extent of oxygenation of the blood in the specified

time interval. The volume of oxygen delivered was then calculated using the following equation:

$$mL O_2 = 1.34 \times Hgb \times \left(\frac{SvO_2}{100} \right) + 0.0031 \times PvO_2, \quad [1]$$

where Hgb is the hemoglobin concentration in grams per deciliter, SvO_2 is the blood saturation, and PvO_2 is the partial pressure of oxygen in the blood (which was ignored). From the above calculation, we determined the maximum volume of oxygen that a 4.5-mL sample of blood can carry at the specific value of Hgb. This volume was divided by the flow rate of the gas from the device to obtain the time interval of infusion needed to raise the SO_2 value to the chosen setpoint. In theory, infusing the oxygen bubbles for the calculated time interval would result in the SO_2 increasing exactly to the corresponding setpoint. In practice, however, instantaneous variability in the output of the mass flow controller, as well as the presence of a small fraction of undissolved bubbles, led to the delivered fraction of oxygen's being less than unity on average. At the end of the experiment, a terminal blood gas analysis was performed to ensure that the high rpm of the stir plate did not affect the hemoglobin concentration in the blood.

The volume of oxygen administered was simply the gas flow rate through the device multiplied by the total time of infusion. The volume of oxygen delivered was calculated using Eq. 1 and the measured increase in SO_2 for the blood volume used. The measurement was performed three times for reproducibility at each gas flow rate. The liquid flow rate was held constant at 12 mL/h since this was the maximum flow employed throughout the study and produced the highest concentration of sub-5- μ m bubbles.

In Vivo Experiments. All procedures were approved by the Institutional Review Board (IRB) at Boston Children's Hospital. For evaluation of the microfluidic device *in vivo*, a rodent model of normoxia was chosen, wherein the oxygen bubbles from the device were infused into the femoral vein of a male Sprague-Dawley rat. Even under conditions of normoxia, the venous system consisting of deoxygenated blood presents a significant oxygen sink for evaluation of the device. To prepare the rat for the infusion, it was placed under anesthesia and fitted with a nose cone for vent-assisted respiration. One angi catheter each was placed in the femoral vein and artery in one leg of the rat. The femoral line was used for infusion of the bubbles. The arterial line was used to draw blood intermittently for monitoring on an arterial blood gas machine. An additional angi catheter was placed in the femoral artery in the other leg of the rat, for placement of pressure transducers which recorded systolic and diastolic blood pressures. To measure the PVR a pressure catheter was placed into the pulmonary artery and a volume-pressure catheter into the left ventricle. Any increase in oxygen tension was measured by means of a pO_2 probe inserted directly into the RV of the heart. The animal was instrumented at an FiO_2 of 100%, following which the FiO_2 was lowered to 30% for a baseline measurement of at least 10 min. At the end of the measurement of baseline variables, the outlet tubing from the device was inserted into the angi catheter in the femoral vein and advanced until the tip was directly in the blood vessel. This procedure ensured that the bubbles were in contact with desaturated blood rather than the inside of the angi catheter upon exiting the tube. The infusion was performed for 30 min, followed by a recovery period of at least 30 min.

Mass Flow Controller Operation. Since gases are compressible, a change in the operating pressure and/or temperature can result in significant changes in their volumetric flow. As a result, a mass flow controller regulates the flow in terms of mass, which is conserved through a flow conduit. The mass flow controller in this study was designed to operate using the units of sccm, indicating standard cubic centimeters per minute, or standard millimeters per minute. When a value of x sccm was specified on the mass flow controller, the instrument regulated flow such that the volumetric flow of gas at its outlet contained the same mass as x mL/min of the gas at the reference conditions for the instrument, which was 101 kPa pressure and 0 °C temperature in the present case. When gas flow occurs at elevated pressures, such as in this study, it is compressed and contains greater mass than an equivalent volume of the same gas at atmospheric pressure. Since the dissolution of oxygen in blood is based on actual mass and not volume, it was imperative that the mass of oxygen delivered through a given volume at any instant be equivalent to that contained in the same volume at reference conditions. Hence, when we refer to a volumetric flow of gas in this paper we are indicating that it was the mass-equivalent of the stated volume of gas at

atmospheric pressure and 0 °C temperature. For example, a stated gas flow rate of 0.25 mL/min at elevated pressures in our experiments indicates that the volume of oxygen delivered was such that it contained the same number of molecules of oxygen as 0.25 mL/min of gas at atmospheric pressure.

Data Availability. All study data are included in the article and/or *SI Appendix*.

ACKNOWLEDGMENTS. We thank Dr. Ravi Thakur and Ms. Faith Thomas for help with the experimental setup. Device fabrication was done with assistance

1. J. N. Kheir *et al.*, Oxygen gas-filled microparticles provide intravenous oxygen delivery. *Sci. Transl. Med.* **4**, 140ra88 (2012).
2. A. T. Lock *et al.*, Interfacial nanoprecipitation toward stable and responsive microbubbles and their use as a resuscitative fluid. *Angew. Chem. Int. Ed.* **57**, 1271–1276 (2017).
3. R. P. Seekell, Y. Peng, A. T. Lock, J. N. Kheir, B. D. Polizzotti, Tunable polymer microcapsules for controlled release of therapeutic gases. *Langmuir* **34**, 9175–9183 (2018).
4. R. P. Seekell *et al.*, Oxygen delivery using engineered microparticles. *Proc. Natl. Acad. Sci. U.S.A.* **113**, 12380–12385 (2016).
5. J. N. Kheir *et al.*, Bulk manufacture of concentrated oxygen gas-filled microparticles for intravenous oxygen delivery. *Adv. Healthc. Mater.* **2**, 1131–1141 (2013).
6. K. J. Black *et al.*, Hemodynamic effects of lipid-based oxygen microbubbles via rapid intravenous injection in rodents. *Pharm. Res.* **34**, 2156–2162 (2017).
7. B. D. Polizzotti, L. M. Thomson, D. W. O'Connell, F. X. McGowan, J. N. Kheir, Optimization and characterization of stable lipid-based, oxygen-filled microbubbles by mixture design. *J. Biomed. Mater. Res. B Appl. Biomater.* **102**, 1148–1156 (2014).
8. J. Li *et al.*, A review on phospholipids and their main applications in drug delivery systems. *Asian J. Pharm. Sci.* **10**, 81–98 (2015).
9. O. Ohgoda, I. N. Robinson, Toxicological evaluation of DSPC (1,2-distearoyl-sn-glycero-3-phosphocholine). *Fundam. Toxicol. Sci.* **7**, 55–76 (2020).
10. K. Hippalgaonkar, S. Majumdar, V. Kansara, Injectable lipid emulsions—advancements, opportunities and challenges. *AAPS PharmSciTech* **11**, 1526–1540 (2010).
11. G. Pu, M. A. Borden, M. L. Longo, Collapse and shedding transitions in binary lipid monolayers coating microbubbles. *Langmuir* **22**, 2993–2999 (2006).
12. Y. Peng *et al.*, Interfacial nanoprecipitation toward stable and responsive microbubbles and their use as a resuscitative fluid. *Angew. Chem. Int. Ed. Engl.* **57**, 1271–1276 (2018).
13. L. M. Thomson, B. D. Polizzotti, F. X. McGowan, J. N. Kheir, Manufacture of concentrated, lipid-based oxygen microbubble emulsions by high shear homogenization and serial concentration. *J. Vis. Exp.* (87): 10.3791/51467. (2014).
14. H. Watanabe, M. Suzuki, H. Inaoka, N. Ito, Ostwald ripening in multiple-bubble nuclei. *J. Chem. Phys.* **141**, 234703 (2014).
15. D. de Fontaine, "Nucleation and growth" in *Principles of Classical Thermodynamics Applied to Materials Science* (World Scientific, 2019), pp. 275–287.
16. K. Sarkar, A. Katiyar, P. Jain, Growth and dissolution of an encapsulated contrast microbubble: Effects of encapsulation permeability. *Ultrasound Med. Biol.* **35**, 1385–1396 (2009).
17. A. Katiyar, K. Sarkar, Stability analysis of an encapsulated microbubble against gas diffusion. *J. Colloid Interface Sci.* **343**, 42–47 (2010).
18. L. M. Thomson, R. P. Seekell, F. X. McGowan, J. N. Kheir, B. D. Polizzotti, Freeze-thawing at point-of-use to extend shelf stability of lipid-based oxygen microbubbles for intravenous oxygen delivery. *Colloids Surf. A Physicochem. Eng. Asp.* **500**, 72–78 (2016).
19. J. N. Kheir *et al.*, Administration of intravenous oxygen increases arterial oxygen content and cerebral oxygen delivery during CCC-only CPR. *Circulation* **126** (suppl. 21), A206 (2012).
20. Z. Li, A. M. Leshansky, S. Metais, L. M. Pismen, P. Tabeling, Step-emulsification in a microfluidic device. *Lab Chip* **15**, 1023–1031 (2015).
21. Y. Peng, J. N. Kheir, B. D. Polizzotti, Injectable oxygen: Interfacing materials chemistry with resuscitative science. *Chemistry* **24**, 18820–18829 (2018).
22. S. A. Peyman *et al.*, Expanding 3D geometry for enhanced on-chip microbubble production and single step formation of liposome modified microbubbles. *Lab Chip* **12**, 4544–4552 (2012).
23. F. W. Tunnicliffe, G. F. Stebbing, The intravenous injection of oxygen gas as a therapeutic measure. *Lancet* **188**, 321–323 (1916).
24. L. Gattinoni *et al.*, COVID-19 pneumonia: Different respiratory treatments for different phenotypes? *Intensive Care Med.* **46**, 1099–1102 (2020).
25. J. O. C. Dunn, M. G. Mythen, M. P. Grocott, Physiology of oxygen transport. *BJA Educ.* **16**, 341–348 (2016).

from Calixto Saenz in the Harvard Medical School Microfluidics Facility, which is supported by NSF Award 1541959. This work was supported by the Office of the Assistant Secretary of Defense for Health Affairs through the Peer Reviewed Medical Research Program under Awards W81XWH-15-1-0544 (J.N.K.) and W81XWH1910237 (B.D.P.). Opinions, interpretations, conclusions, and recommendations are those of the author and are not necessarily endorsed by the Department of Defense. Further, it was supported by the National Institute of Heart, Lung, and Blood Institute (1R01HL141818-02, B.D.P.) and a DRIVE grant from the Boston Biomedical Innovation Center (NIH U54HL119145, B.D.P.).